Weierstraß-Institut
für Angewandte Analysis und Stochastik

im Forschungsverbund Berlin e.V.

Preprint ISSN 0946 – 8633

A comparison of analytical cutting force models

Oliver Rott[1], Dietmar Hömberg[1], Carsten Mense[2]

submitted: July 11, 2006

[1] Weierstrass Institute
for Applied Analysis and Stochastics
Mohrenstr. 39
10117 Berlin
Germany
E-Mail: rott@wias-berlin.de
hoemberg@wias-berlin.de

[2] Institute for Machine Tools and
Factory Management
Technical University Berlin
Pascalstrasse. 8-9
10587 Berlin
Germany
E-Mail: mense@iwf.tu-berlin.de

No. 1151
Berlin 2006

2000 *Mathematics Subject Classification.* 70E50, 70J25.

Key words and phrases. Milling, regenerative chatter, time domain simulation, stability, machine dynamics.

This work has been supported by DFG-SPP1180 of Deutsche Forschungsgemeinschaft.

Edited by
Weierstraß-Institut für Angewandte Analysis und Stochastik (WIAS)
Mohrenstraße 39
10117 Berlin
Germany

Fax: + 49 30 2044975
E-Mail: preprint@wias-berlin.de
World Wide Web: http://www.wias-berlin.de/

Abstract. The modeling of dynamic processes in milling and the determination of stable cutting conditions have become increasingly important for the optimization of manufacturing processes. Analytic approaches and time domain simulations based on simplified dynamic systems are used to identify chatter-free machining conditions. Stresses applied to the system are generally estimated by cutting force models. The goal of this paper is to compare the influence of the cutting force models on the stability limits. Numerical simulations of a simplified, generic milling machine model are therefore performed, while varying the cutting force approach. In order to distinguish stable from unstable cutting conditions a numerical stability criterion is used. The resulting stability charts are then investigated and analyzed to show the effect of the different cutting force models.

1. Introduction

The productivity of metal cutting processes is among other effects limited by the occurrence of chatter. The arising vibrations of the cutting tool lead to poor surface finish of the machined workpiece and the machine wears out rapidly. Although chatter is caused by several physical mechanisms, the regenerative effect is considered to be the most important reason for unstable cutting conditions. Hence this effect has been widely studied since the late 1950s by several authors, e.g. Tobias and Fishwick [20], Tlusty [19], Altintas [1], Stépán [17] and Weck [22]. Their research has shown that the regenerative effect is based on the modulation of the cutting force due to the relative movement of workpiece and cutting tool, which finally leads to self-excited vibration.
In milling, depending on the cutting conditions such as spindle speed, axial depth of cut and radial immersion, these vibrations can either decay and produce a stable cut, or grow in an unstable manner to result in chatter. Some authors assume that the feed per tooth does not influence the stability [1], while others observe an effect on the stability limit [3]. However, using the parameters spindle speed and axial depth of cut, the borderline between stable and unstable cut can be depicted in a stability lobes diagram (SLD), which helps in practice to find the optimal cutting conditions.
The accurate prediction of chatter needs complex dynamic models including a detailed description of the cutter geometry, a precise cutting force model, a machine model with many degrees of freedom and eventually a dynamic model for the workpiece. However, for the sake of simplicity many authors investigate reduced models, which provide acceptable results in several special cases, e.g. Altintas [1], Faassen [3], Insperger and Stépán [8] and Li [12]. The relation between displacement, feed per tooth and resulting cutting force is either described with an approach based on perfect plasticity, e.g. Oxley [13] and Li [10, 11], or with an empirical cutting force model. Since the construction of SLDs needs many evaluations of the underlying differential equation, it is more effective to use empirical models allowing for a cutting force calculation without great numerical effort. A vast number of cutting force models can be found in literature. They may be linear or non-linear and some have an additional constant term representing the edge forces. Accordingly, the structure of the differential equation describing the system dynamics depends on the selected cutting force model. In turn this might affect the SLDs. Hence, the goal of this paper is to analyze the relation between cutting force model and SLD in detail.

A straightforward way to calculate SLDs for all types of cutting force models is to apply a time domain simulation method (which is done here with the Matlab dde23 solver) in

connection with a chatter criterion to distinguish stable from unstable cutting conditions. The result of each calculation may then be used to determine a point in the SLD. Finally the results can be compared with each other to figure out the effect of the cutting force model on the stability of the milling system, described by a delay differential equation.
Section two deals with the mathematical model of the considered milling system and gives a summary of the most common cutting force models, followed by a demonstration of how the constants in the cutting force models can be determined from experimental data. In Section 3 a simulation tool is developed and validated by comparison with other techniques. In Section 4 the results of the calculation are compared with each other in order to work out the differences. Finally the results are summarized.

2. Modeling

2.1. **Machine Model.** The milling process can be represented schematically by a turning cutter removing material from the workpiece, the latter translating in the direction of feed as depicted in Fig. 1.

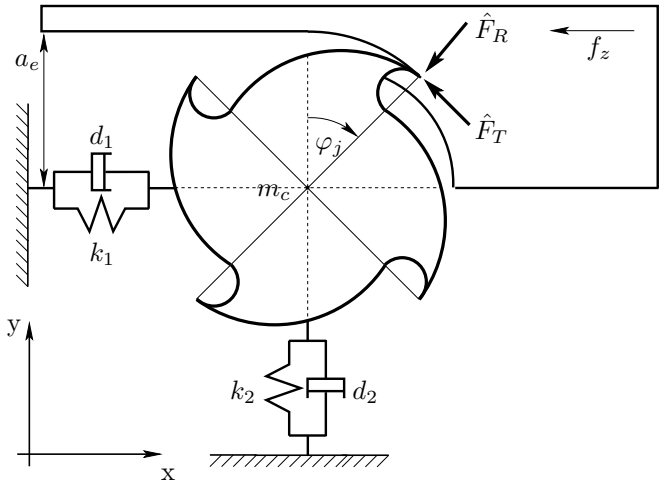

Figure 1: Schematic representation of the milling process.

The machine and the attached cutter are modeled as a two degree of freedom (2DOF) oscillation system, where the mass m_c of cutter and machine is concentrated in the center point. Although this is a simplified milling machine model, which cannot reproduce more than two eigenfrequencies of a real milling device, it is sufficient to consider this system to show the effect of the different cutting force models. According to Newton's second law the equation of motion for this system reads:

$$\ddot{u} + \begin{bmatrix} 2\xi_1\omega_1 & 0 \\ 0 & 2\xi_2\omega_2 \end{bmatrix} \dot{u} + \begin{bmatrix} \omega_1^2 & 0 \\ 0 & \omega_2^2 \end{bmatrix} u = \frac{1}{m_c} F \,, \tag{2.1}$$

where the Eigen angular frequencies in x- and y-direction are denoted by $\omega_i = 2\pi f_i = \sqrt{\frac{k_i}{m_c}}$. The modal damping in each direction is represented by $\xi_i = \frac{d_i}{2m_c k_i}$. The right hand side of

eq. (2.1) takes into account the cutting force $F = [F_x, F_y]^T$ acting on each tooth in cut. The decision whether a tooth is cutting or not is taken with the help of a screen function introduced by Insperger et al. [7]:

$$g(\varphi_j) = \begin{cases} 1, & \varphi_{st} \leqslant \varphi_j \leqslant \varphi_{ex}, \\ 0 & \text{otherwise} \end{cases} \tag{2.2}$$

Here, φ_{st} and φ_{ex} are the starting and exit angle for one flute j. For example, in Fig. 1 $\varphi_{st} = 0$ and $\varphi_{ex} = \frac{\pi}{2}$. Using the function g, the right hand side can be written as:

$$F = \sum_{j=0}^{N_z-1} \underbrace{a_p g(\varphi_j) O(\varphi_j)}_{A^j(t)} \frac{1}{a_p} \hat{F} \tag{2.3}$$

with

$$O(\varphi_j) = \begin{bmatrix} -\sin\varphi_j & -\cos\varphi_j \\ -\cos\varphi_j & \sin\varphi_j \end{bmatrix},$$

where N_z is the number of tooth and a_p is the axial depth of cut. $\hat{F} = [\hat{F}_R(h), \hat{F}_T(h)]^T$ represents the radial and tangential cutting force acting on the tip of each flute. The angle of the tooth "j" is calculated as shown by Altintas [1]:

$$\varphi_j(z) = \varphi + j\frac{2\pi}{N_z} - \frac{2\tan\beta}{D} z, \quad \text{with } \varphi = \frac{2\pi N}{60} t \tag{2.4}$$

and spindle speed N in rpm. To simplify the exposition, in the sequel we assume the helix angle β to be zero. This implies that the z-direction need not be taken into account in eq. (2.1).

Finally the system parameters have been chosen, such that the selected values could correspond to the lowest eigenvalues of a real machine. The eigenfrequencies $f_i = 100$Hz and the modal damping $\xi_i = 0.2\%$ are assumed to be the same in each direction. The mass has been chosen to be $m_c = 20kg$.

2.2. **Cutting force models.** Most of the empirical cutting force models can be written as

$$\hat{F} = \mathcal{F}(h, a_p). \tag{2.5}$$

This means that the cutting forces are a function of the chip thickness h and the axial depth of cut a_p. During a milling operation the workpiece is pushed with the feed per tooth f_z in the direction of the cutter, which rotates with the spindle speed N. The cutter then tries to cut a chip with the corresponding approximate static chip thickness $h_{stat} = f_z \sin\varphi_j$, which generates a force applied to the cutter. The applied force induces a displacement of the cutter and, according to the Eigen frequencies of the milling system, a wavy surface is generated. The following flute oscillates because of the induced motion of the cutter and cuts into a wavy surface produced by the tooth before. So the chip thickness consists of a static and a dynamic part: $h = h_{stat} + h_{dyn}$. The dynamic chip thickness is determined by the actual position of the cutting tooth and by the position of the tooth one period $\left(\tau = \frac{1}{NN_z}\right)$ before:

$$h_{dyn} = \big[u(t) - u(t-\tau)\big] e_j, \tag{2.6}$$

with $e_j = [\sin\varphi_j, \cos\varphi_j]^T$ the unit vector in radial direction corresponding to φ_j.

If the chip thickness $h = h_{stat} + h_{dyn}$ becomes negative, the flute is out of cut and no force is acting on the cutter. One can express this condition with the maximum function:

$$h_+ = \max(h, 0) = \begin{cases} h & \text{if } h > 0, \\ 0 & \text{otherwise,} \end{cases} \tag{2.7}$$

which induces a non-linearity in the computation of the cutting forces. In the case of linear models (Weck, Altintas) the usage of the positive part function is not mandatory, since one can evaluate the cutting force expression even for h negative. The situation is different for non-linear models (Stépán, Faassen, Kienzle-Victor), because the exponent of h is in $(0, 1]$. Thus, the cutting force cannot be computed for negative values of h and it is necessary to use h_+ instead of h. A number of different cutting force models can be found in literature. A widely used approach is described by Weck [22]. Here, the cutting force is proportional to axial depth of cut and chip thickness:

$$\hat{F} = K a_p h, \tag{2.8}$$

where $K = [K_R, K_T]^T$ denotes the specific cutting force. This constants depend on the cutting speed and have to be determined experimentally. Altintas [1] extended this approach. He introduced edge forces to account for the contribution of friction for $h = 0$ mm to the cutting force:

$$\hat{F} = K a_p h + K_e a_p. \tag{2.9}$$

Another possibility is to use a non-linear relation between cutting force and chip thickness, as was proposed by Tobias [20] or Stépán [17]:

$$\hat{F} = K a_p h_+^{x_f}. \tag{2.10}$$

In this approach $x_f \in (0, 1]$ is another empirical parameter. An attempt which allows a better representation of experimental data was developed by Kienzle and Victor in the early 1950s. This approach is described in detail by Tönshoff & Denkena [21]:

$$\hat{F}_i = \tilde{K}_i(h_+) a_p h_+, \tag{2.11}$$

$$\tilde{K}_i = \begin{cases} k_i^3 h_+^{-m_i^3} & , 10^{-3}\text{mm} \leqslant h_+ \leqslant 10^{-2}\text{mm} \\ k_i^2 h_+^{-m_i^2} & , 10^{-2}\text{mm} < h_+ \leqslant 10^{-1}\text{mm} \\ k_i^1 h_+^{-m_i^1} & , 10^{-1}\text{mm} < h_+ \leqslant 1\text{mm} \end{cases}.$$

The large number of free parameters allows for a cogent reproduction. Faassen [3] presents a combination of the models shown above. He proposes an extension of Stépán's model by edge effects introduced by Altintas:

$$\hat{F} = K a_p h_+^{x_f} + K_e a_p. \tag{2.12}$$

In Table 1, the models to be discussed are summarized.

Model	Weck	Altintas	Stépán	Kienzle & Victor	Faassen
eq. no.	(2.8)	(2.9)	(2.10)	(2.11)	(2.12)
linear	x	x			
non-linear			x	x	x
edge coefficients		x			x

Table 1: Summary of the cutting force models to be compared.

2.3. **Experimental determination of the cutting constants.** Every model presented above, contains free parameters which are determined with the help of experimental data. For this purpose machining tests were performed with the material AlZn6Mg2Cu2Zr an aluminium alloy with the material number AA7050. The cuts have been made using a 5 axis milling machine from A&B MAP, Berlin type LPZ 500. For the experiments a carbide end mill with 15 mm diameter, three cutting edges, a chip angle of 14°, a clearance angle of 10° and a spiral angle of 30° was used. The end mill was fixed in a heat shrinking toolholder with a HSK-A mounting shank according to DIN 69 882-8. A schematic representation of the experimental setup is shown in Fig. 2. The workpiece is mounted on a 3-component dynamometer type Kistler 9257B that is connected to three charge amplifiers type Kistler 5011. For data acquisition a measuring board from National Instrument with a maximum sampling rate of 500 kHz and a resolution of 16 bit was used.

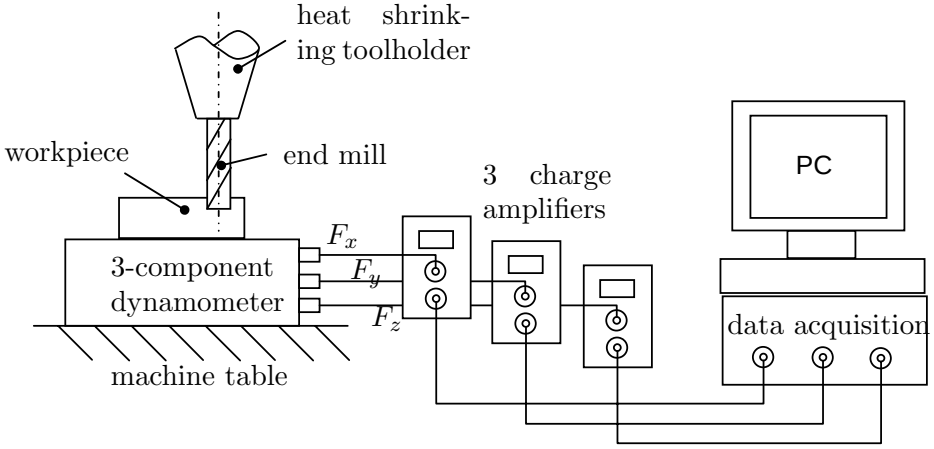

Figure 2: Experimental setup for determining the cutting forces

The data logging has been done with a sampling rate of 20 kHz. The cutting speed has been varied from 100 m/min to 400 m/min which correspond approximately to a spindle speed of 2122 rpm up to 8488 rpm. At each spindle speed, the feed per tooth has been varied form 0.05 mm/tooth to 0.45 mm/tooth with increments of 0.05 mm/tooth. The cutting depth has been varied form 2 mm to 6 mm with increments of 2 mm. From the experimental data we

computed the cutting constants using a least squares method as described in [1, Sec. 2.8.1]. To this end the measured cutting forces $F^{exp}(t_i)$ at discrete times t_i has been averaged over one tooth period, i.e.

$$\bar{F}^{exp} = \frac{1}{\tau} \int_0^{\tau} F_x^{exp}(t) dt$$

These average values, assuming a rigid machine, can also be expressed by the analytical cutting force (cf. eq. (2.3)), averaged over one tooth period (with spacing angle $\varphi_p = \frac{2\pi}{N_z}$):

$$\bar{F}(f_z) = \frac{1}{\varphi_p} \int_{\varphi_{st}}^{\varphi_{ex}} F(h_{stat}, f_z)\, d\varphi. \tag{2.13}$$

Thus, both averaged expressions can be used to construct a functional describing the distance between the calculated and measured forces for several feed per tooth:

$$J(K_i) = \sum_{j=1}^{m} \left[\bar{F}_i^{exp}(f_z^j) - \bar{F}_i(f_z^j) \right]^2. \tag{2.14}$$

The minimization of this functional with constraints (all exponents have to be in the interval $[0, 1]$, for the Kienzle-Victor model additional continuity assumptions are required) yields an optimal set of parameters K_i and exponents x_f, m_i^{α}. Hence the presented technique allows adjusting each cutting force model to a set of experimental data. The results of the optimization process are summarized in Tables 2 and 3. The minimum value of the objective functional is given in the last row. It indicates the accuracy of each fit of the measured data. It is obvious that, depending on the analytical form of the cutting force model, the approximation of the experimental mean cutting forces is more or less accurate. Therefore a certain error is already introduced at this stage. This means, that for given chip thickness and immersion each cutting force model yields a slightly different force in x,y-direction (cf. eq. (2.3)), which may affect the stability limit.

	Weck	Altintas	Stépán	Faassen
K_R	596 $\frac{N}{mm^2}$	346 $\frac{N}{mm^2}$	289 $\frac{N}{mm^{1+x_f}}$	273 $\frac{N}{mm^{1+x_f}}$
K_T	1093 $\frac{N}{mm^2}$	839 $\frac{N}{mm^2}$	607 $\frac{N}{mm^{1+x_f}}$	719 $\frac{N}{mm^{1+x_f}}$
K_{Re}	–	31 $\frac{N}{mm^2}$	–	28 $\frac{N}{mm^2}$
K_{Te}	–	50 $\frac{N}{mm^2}$	–	29 $\frac{N}{mm^2}$
x_f	–	–	0.63	0.82
J^{min}	80711.7 N	1602.9 N	7916.4 N	729.8 N

Table 2: Summary of determined cutting constants for the models of Weck, Altintas, Stépán and Faassen

	$0.001 < \tilde{h} < 0.01$	$0.01 \leq \tilde{h} < 0.1$	$0.1 \leq \tilde{h} < 1$
k_R^i	39	99	298
k_T^i	336	493	667
m_R^i	1.0	0.8	0.32
m_T^i	0.53	0.45	0.32

Table 3: Summary of determined cutting constants for the model of Kienzle/Victor, J^{min}=383 N ($\tilde{h} = h/h_0$, h_0=1mm, k_R^i and k_T^i are given in $N/mm^{1-m_r^i}$ and $N/mm^{1-m_t^i}$).

3. Stability analysis

3.1. **Time-domain-simulation versus Floquet theory.** The dynamic chip thickness (2.6) induces a constant delay in the equation of motion (2.1), hence it can be rewritten in the following abstract form:

$$\begin{aligned} y'(x) =& f(x, y(x), y(x-\tau)), \\ y_0(\sigma) =& \Phi(\sigma) \quad \sigma \in [-\tau, 0]. \end{aligned} \tag{3.1}$$

In order to analyze the stability of a periodic solution ($y(t+T) = y(t)$), one may linearize (3.1) and apply results from Floquet theory for delay differential equations (DDEs). As described in [6, 7] this approach allows for a fast and accurate construction of SLDs, based on a well-defined stability criterion. Moreover, the computed stability characteristics don't depend on the initial conditions.

On the other hand it gives no information about the temporal evolution of the models and the quality of the machined surface. A way to avoid this drawbacks is to apply a time-domain simulation algorithm on (3.1). Unfortunately the computing time is much higher than for the previous method. But time domain simulation is very easy to implement and the incorporation of non-linear terms is straightforward. Depending on the time discretization, it results in a fine temporal resolution of the solution, thereby implicitly yielding information about the structure of the machined surface. (3.1) can be solved in several ways. Campomanes [2] and Sims [15] apply a solver for ordinary differential equations in combination with a dedicated algorithm to compute the dynamic chip thickness from the amount of material cleared away from the workpiece. This can also be computed using the CSG-method as shown by Suhrmann [18]. On the one hand, these methods solve the problem offering at the same time a detailed representation of the machined surface, on the other hand, dealing with all this information is quite demanding in terms of storage capacity and computing power. Eventually we have decided a direct tackling of the DDE (3.1) by using the Matlab solver dde23. For details about this Runge-Kutta based algorithm we refer to [14].

3.2. **A chatter criterion.** Once a transient solution for fixed initial conditions has been obtained, it is necessary to decide whether the solution is stable or not. This can be done with a chatter indicator. Sims [15] presents a criterion which uses Fourier analysis of the data to distinguish oscillations due to separate excitation from those due to self excitation. Thus it is possible to judge whether the amplitude of self exited vibrations decays or increases.

In the case of increase the state is identified as unstable. Li [12] proposes another chatter indicator, comparing the dynamic cutting force with the static one. Campomanes [2] makes use of a similar indicator, but he considers directly the dynamic and static chip thickness. In order to obtain such a dimensionless chatter indicator, either the cutting force or the chip thickness is taken to compute the maximum value of the static and dynamic quantity over several revolutions of the tool. The maximum resulting from the dynamic quantity is then divided by the maximum of the static quantity. This renders the number searched for, which may be denoted as follows:

$$\eta = \frac{\max(|F_{dyn}|)}{\max(|F_{stat}|)} \tag{3.2}$$

or

$$\eta = \frac{\max(h_{dyn})}{\max(h_{stat})}. \tag{3.3}$$

If η is greater than a certain threshold value η^{th}, the solution is considered to be unstable. If $\eta \leq \eta^{th}$, the solution is stable. However, there is no general agreement on where the threshold lies. Li recommends the use of $\eta^{th} = 1.3$. Campomanes identifies a value $\eta^{th} = 1.25$. Sims, who investigates the chatter indicator η as well, suggests a threshold value $\eta^{th} = 1.05$. However, for large simulation times and homogenous initial conditions a threshold $\eta^{th} = 1$ should yield the correct stability limit.

Another method to classify the results of the time domain simulation was introduced by Smith and Tlusty [16]. They use a peak to peak (PTP) forces scheme to identify stable cutting conditions.

Here we compute the solution to (2.1) with matlab dde23 solver, while the chatter indicator developed by Li (3.2) is used to identify the stable system states. The resulting algorithm is summarized in the following scheme:

- Choose iteration parameters $n > k \geq N_z$ and $\eta^{th} \geq 1$;
- Solve problem (2.1) for the time interval $(t_0, t_E = n\tau]$, where $\tau = \frac{1}{NN_z}$;
- Calculate η according to (3.2) for $t \in [t_E - k\tau, t_E]$;
  - if $\eta > \eta^{th}$, the system state is unstable;
  - if $\eta \leq \eta^{th}$, the system state is stable;
- Vary a_p and recalculate η until the stability limit is approximated sufficiently well.

However, all the above presented techniques and the algorithm chosen here have an obvious drawback. Furthermore the stability limit depends on the number of simulated revolutions of the tool [15]. Hence, the parameter n must be carefully chosen, while the choice of k is rather uncritical.

3.3. **Validation of the numerical algorithm.** Before we can apply our approach to the different cutting force models, we have to clarify the role of the iteration parameter. To this end we have to study the asymptotic behavior with respect to growing n and the choice of η^{th} for fixed spindle speed $N = N_0$. Moreover, the dde solver provides the possibility to adjust the admissible relative error of the numerical solution (cf. [14]). In the computation of the asymptotic behavior of the stability limit the admissible relative error has been set to 10^{-4}.

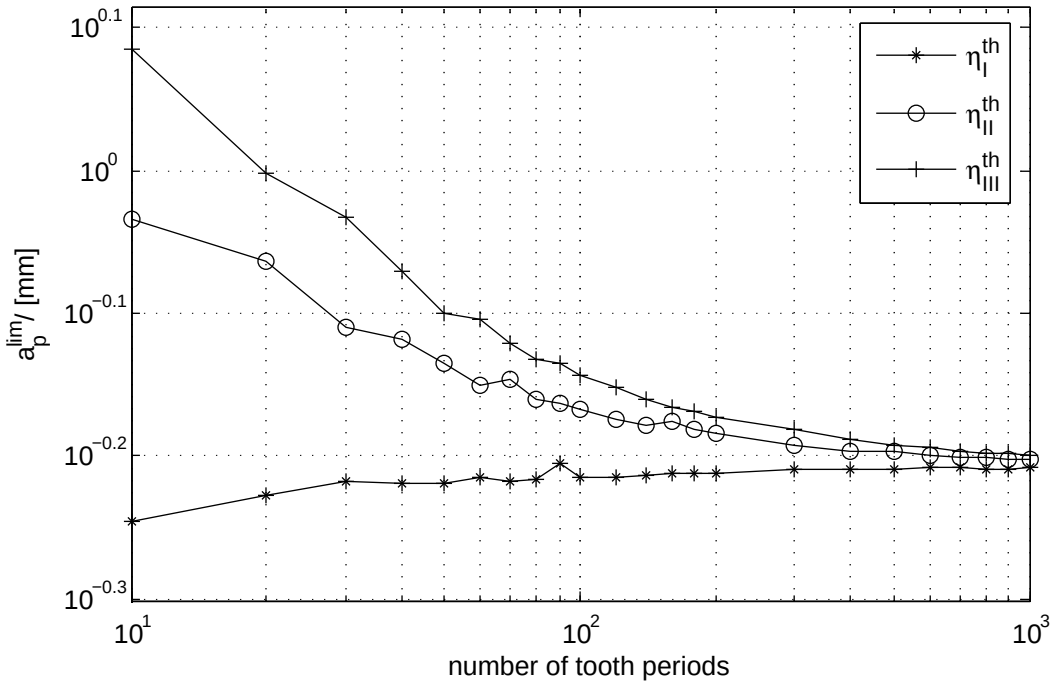

Figure 3: Convergence of the stability limit in 1D.

To validate the time domain method, we compare the limit value a_p^{lim} with the stability limit predicted by the Floquet theory used by Insperger [6, 8]. For the reader's convenience, we summarize this approach in the Appendix.

threshold value	stab. limit / [mm]
$\eta_I^{th} = 1$	0.62
$\eta_{II}^{th} = 1.2$	0.627
$\eta_{III}^{th} = 1.4$	0.632

Table 4: Comparison of asymptotic stability limits.

We begin with the stability limit of a one dimensional system investigated by Insperger [6], who uses the machine parameters f_n=146.5 Hz, $\xi = 0.32$ % and m_c = 2,573 kg. A linearization of Stépán's cutting force model yields the cutting forces acting on the cutter. The cutting constants are $K_T = 10^8 N/mm^{1+xf}$, $K_R = 0.3K_T$ and $xf = 0.8$. The investigated up-milling process with single tooth cutter has entry and exit angles of φ_{st}=0 $\varphi_{ex} = 58.26°$. For a spindle speed $N_0 = 3400$ rpm the updated semi-discretization method (see Appendix) yields a stability limit $a_p^{lim} = 0.59$ mm for a discretization parameter $m = 80$. In order to test our algorithm, a series of numerical experiments have been done. For the same fixed rotation speed as above, the stability limit a_p^{lim} was computed for 10 up to 1000 revolutions of the cutter. This was done for three different threshold values of the chatter indicator: $\eta_I^{th} = 1$, $\eta_{II}^{th} = 1.2$ and $\eta_{III}^{th} = 1.4$. The convergence results are depicted in Fig. 3. The

obtained asymptotic stability limits in terms of a_p are summarized in Table 3.3. As one can see our approach yields a slightly higher stability limit. As aspected the best results are achieved with the threshold η_I^{th}. From a simulated time of 200τ up to 1000τ the calculated stability limits are almost constant and approximately equal to the asymptotic value. However, since the computing time increases markedly with the number of simulated rotations, we restricted the simulation time to 300τ, which seems to be an acceptable compromise between computing time and accuracy. Unfortunately, this choice of simulation time cannot be generalized. Depending on the considered dynamical system (eigenfrequencies, modal damping etc.) one observes different convergence rates of the stability limit. After having determined the simulation parameters a SLD can be computed. According to Insperger we consider spindle speeds in the range of 2800 rpm up to 4000 rpm. The resulting SLDs of both methods are given in Fig. 4.

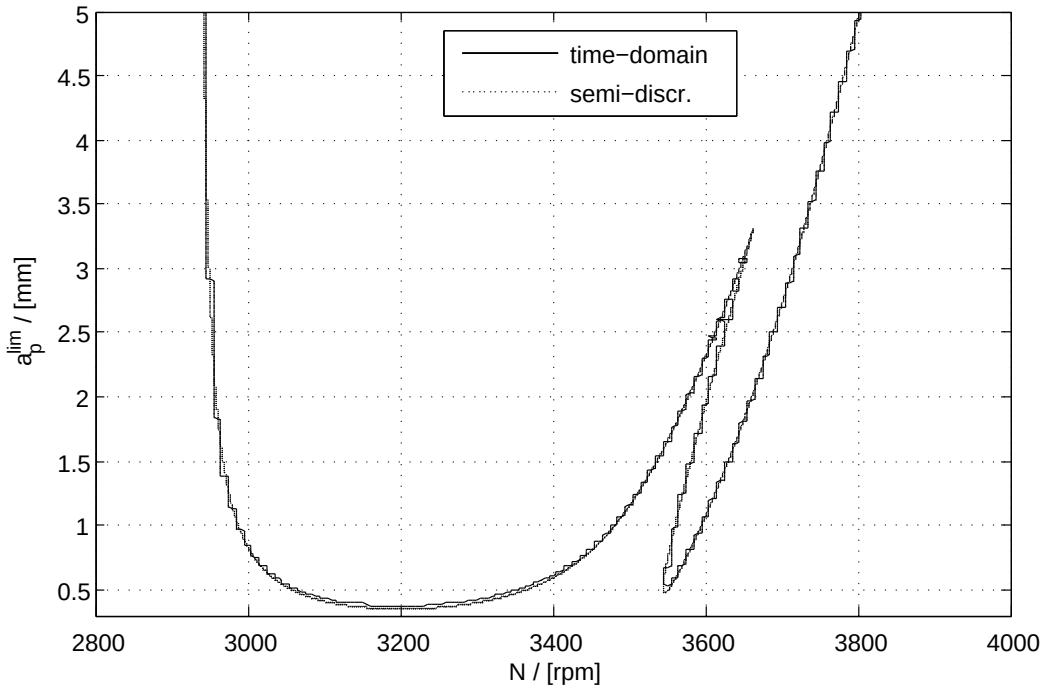

Figure 4: Comparison of semi-discretization and time domain simulation on the basis of a 1D milling system.

We observe that the time domain simulation results are in good agreement with those computed by Insperger's approach.

As a second example we consider a two dimensional milling system as described by Insperger [8]. The parameters of the treated system are (the values in x- and y-direction are the same): eigenfrequency $f = 922$ Hz, damping ratio $\xi = 1.1$ % and mass $m_c = 0.03993$ kg. The cutting force model was chosen according to Weck, with cutting constants $K_t = 6{\cdot}10^8 \frac{N}{m^2}$ and $K_n = 2{\cdot}10^8 \frac{N}{m^2}$. A two fluted cutter was used here. For a spindle speed $N_0 = 15000$ rpm, for full immersion cutting and for a discretization parameter $m = 40$ Insperger [8] obtains a stability limit $a_p^{lim} = 0.1144$ mm. In Fig. 5 the stability limit is shown with respect to the simulated tooth periods.

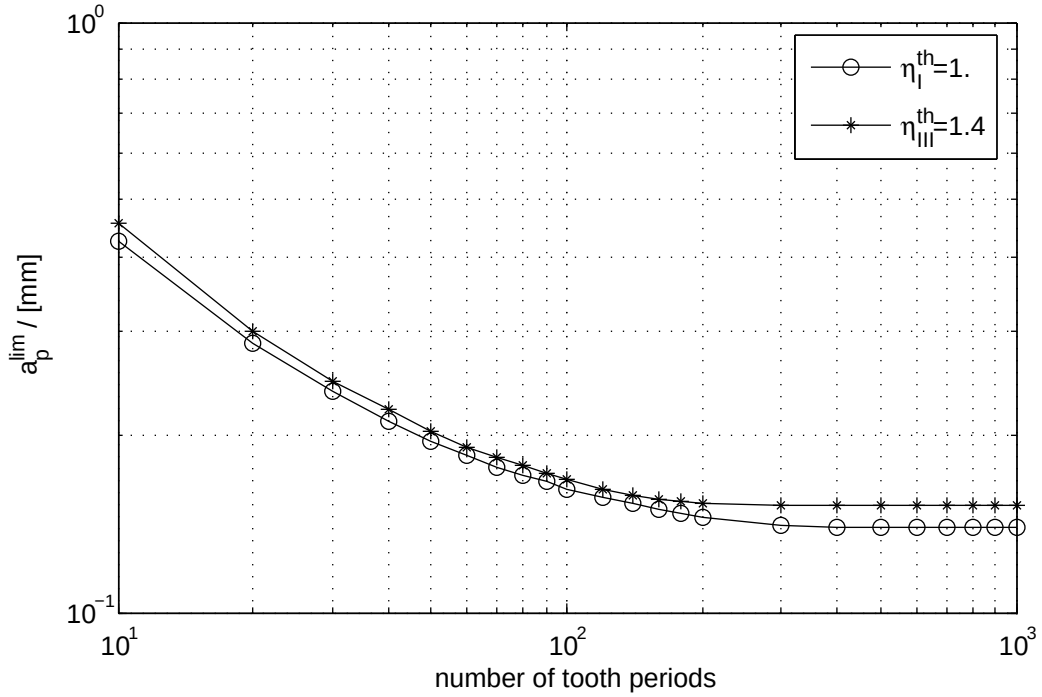

Figure 5: Convergence of the stability limit in 2D.

The graph is similar to the 1D case depicted in Fig. 3. Again, the diagram shows that the threshold $\eta_I^{th} = 1$ is the most appropriate. Using this threshold the calculated asymptotic stability limit is from a simulation time of 150 up to 1000 tooth periods approximately constant. The final value is $a_p^{lim} = 0.1391$ mm. Hence we restricted the simulation time for this problem to 150 tooth periods. The results are in good agreement with Insperger's method as one can see in Fig. 6. Fig. 6 confirms again the former assessment that the stability limit computed by the time domain simulation is higher. Furthermore, the distance between the curve computed with semi-discretization and the one calculated with time domain simulation is slightly with increasing spindle speed. But aside from this both methods yield the same SLD.

The comparison with an independent stability analysis techniques shows that our time domain simulation algorithm provides reliable results. The threshold was determined to be $\eta^{th} = 1$. Using this threshold, the error remains – especially for long simulation runs – within an acceptable range. Nevertheless, since the final results depend on the number of simulated tooth periods, it is always helpful to estimate the minimum simulation time by means of a convergence test, as shown in Fig. 3 and Fig. 5. Having performed these tests, the time domain algorithm can be used to compute the SLDs for arbitrary cutting force models. This finally allows a comparison of linear and non-linear cutting force models in terms of the predicted stability limit, which one can use in turn to estimate the effect of the non-linearities, as we show in the following section.

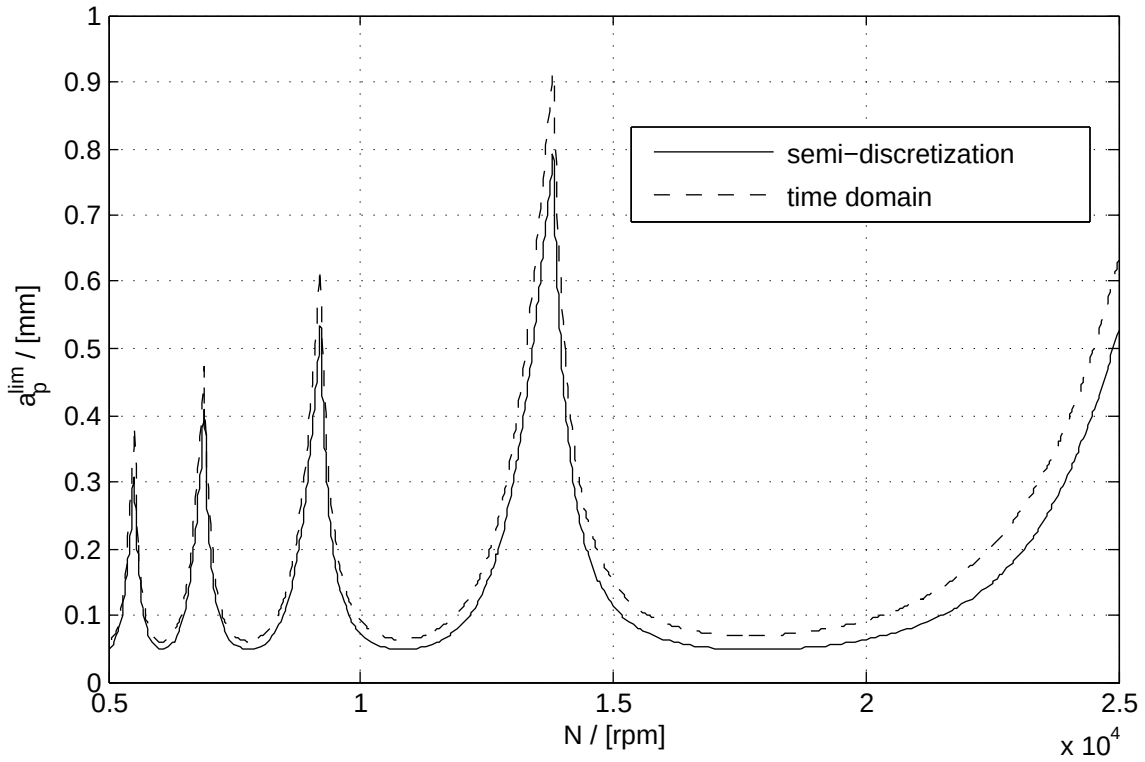

Figure 6: Comparison of semi-discretization and time domain simulation on the basis of a 2D milling system.

4. Comparison of cutting force models

4.1. **Preliminaries, estimation of simulation time.** The basis for the comparison of the presented cutting force models is the simple machine model imposed in Section 2.1. In order to investigate the effect of each cutting force approach, only the right hand side of the resulting equation of motion (2.1) is modified. The right hand side, which is given by expression (2.3), includes a force vector $[\hat{F}_R, \hat{F}_T]^T$, that we choose according to one of the analytical cutting force models introduced in Section 2.2. Then we compute the respective stability chart for at least two values of the feed per tooth.
In principle, the given procedure allows to get an impression of how the stability lobes diagram changes with the cutting force model. However, the computed charts contain an additional error due to the computation of the cutting constants. Since the accuracy of the approximation of the experimental data (cf. the residual J^{min} in Tables 2 and 3) varies with each cutting force model, the differences may become visible in the final results. In the following we suppose that the effect of this error is small in comparison to the differences resulting from the analytical form of the cutting force models.

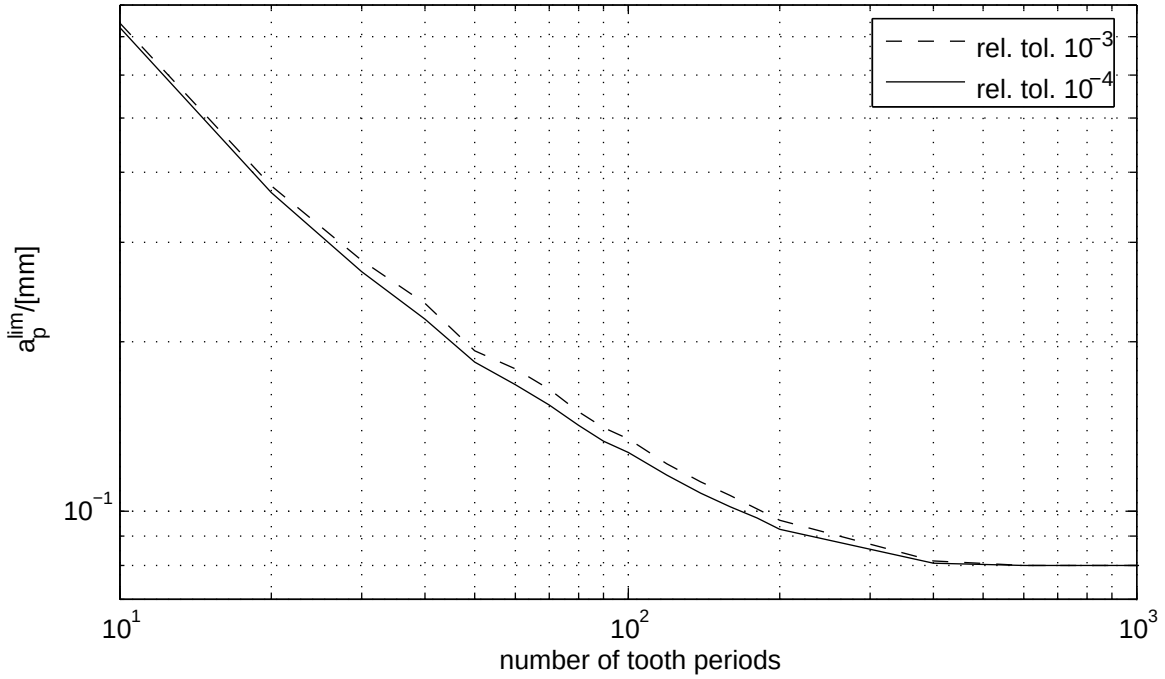

Figure 7: Convergence of the stability limit for $f_z = 0.05$ mm.

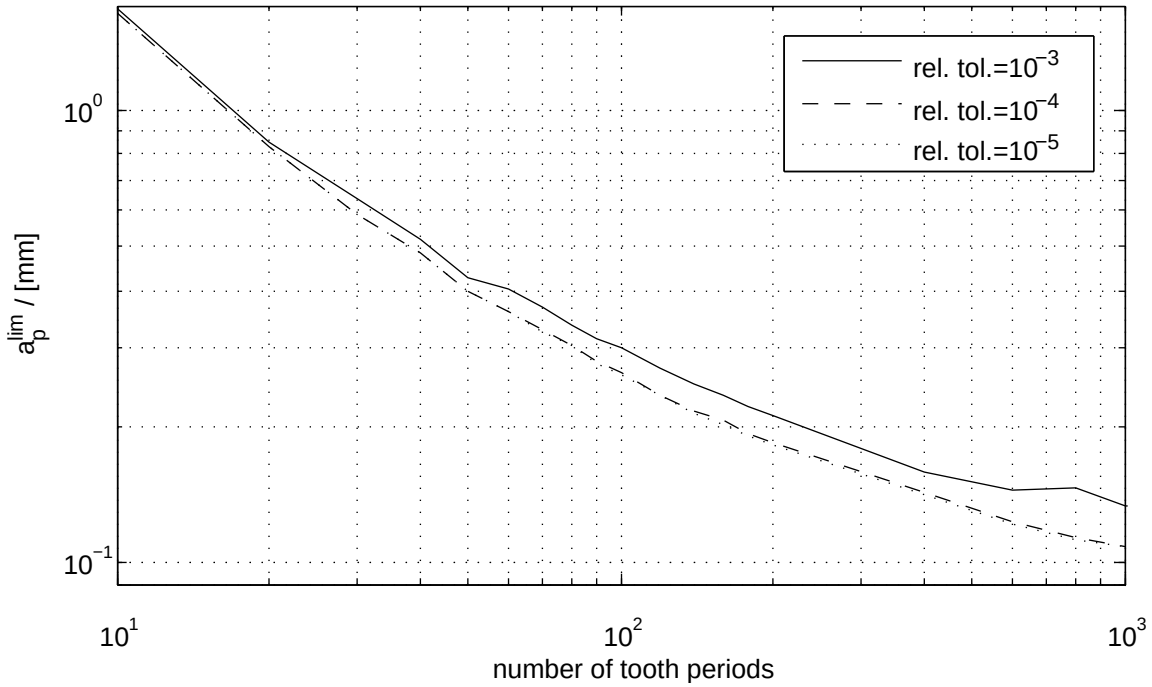

Figure 8: Convergence of the stability limit for $f_z = 0.45$ mm.

The first step for the computation of the stability charts is the estimation of the simulation time, as described in Section 3. Since the estimated simulation time is uniformly fixed for every cutting force model, we perform the convergence tests for Stépán's non-linear model, assuming this model has the worst convergence characteristics. In order to get an idea of the effect of the feed per tooth, we investigated the asymptotic behavior of the system for $f_z = 0.05$ mm and for $f_z = 0.45$ mm. The spindle speed was fixed to 1200 rpm. The result of the convergence test applying a threshold $\eta^{th} = 1$ to identify the stable cutting conditions is depicted in Fig. 7 and 8. Fig. 7 shows that the stability limit for $f_z = 0.05$ mm remains approximately constant for simulation times greater than 400 tooth periods. Moreover the convergence is mesh independent for the chosen parameters. A reduction of the admissible relative error of the numerical solution from 10^{-3} to 10^{-4}, leading to smaller time steps, does not improve the convergence result markedly. For $f_z = 0.45$ mm (cf. Fig. 8) we observe a different behavior of the stability limit. Here, the convergence curve becomes smoother and the stability limit decreases when the admissible relative error is reduced from 10^{-3} to 10^{-4}. A reduction form 10^{-4} to 10^{-5} brings no further improvement as the third curve shows. Thus, we state mesh independence for an error limit smaller than $10^{-}4$. This does not only demonstrate the essential role of the simulation time for precise results, but also that of error control during the numerical solution of the DDE. As the second curve for $f_z = 0.45$ mm does not show the same convergence characteristics as the curve for $f_z = 0.05$ mm, it is difficult to determine the optimal simulation time, which in this case must be greater than 900 tooth periods. Such simulation times are not practicable. In order to be able to compare the results for $f_z = 0.05$ mm and $f_z = 0.45$ mm we have chosen a simulation time of 501 tooth periods according to the convergence characteristic for $f_z = 0.05$ mm, accepting a greater error of the result for $f_z = 0.45$ mm.

4.2. **Comparison of the linear and non-linear models.** After having determined the simulation time, we compute the stability lobes diagrams for every cutting force model varying the feed per tooth. The stability limits for the models of Weck and Altintas can be computed using either the chip thickness h or the positive part of the chip thickness h_+. The latter transforms originally linear models into non-linear ones. This might change the stability limit calculated for these models. In order to display this effect we computed the stability charts for Altintas's model using h as well as h_+ and compared them.

The results for $f_z = 0.05$ mm and $f_z = 0.45$ mm are depicted in Figs. 9 and 10 (here for reasons of clarity, we only displayed the results of Altintas's model for h_+). In both figures the stability limit is given with an accuracy of $\pm$ 0.01 mm. It is obvious that all cutting force models predict stability peaks for spindle speeds N_1=2000 rpm, N_2=1000 rpm, N_3=666.67 rpm, N_4=500 rpm and N_5=400 rpm. These are the natural stability maxima resulting from the eigenfrequencies of the oscillation system and from the tooth number of the cutter.

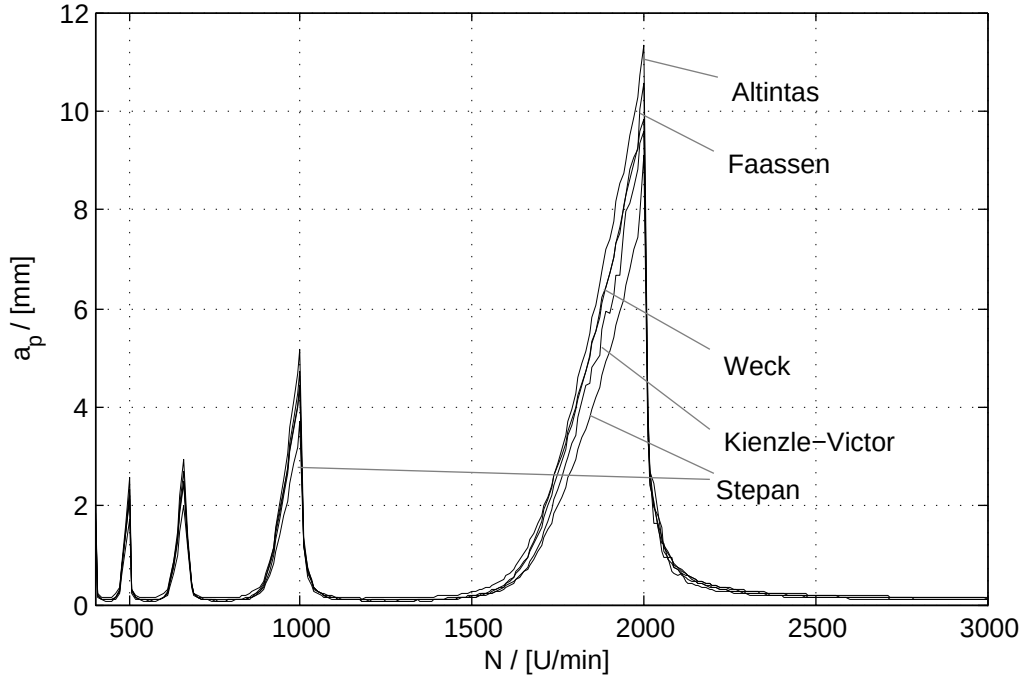

Figure 9: Comparison of the stability charts for $f_z = 0.05$ mm.

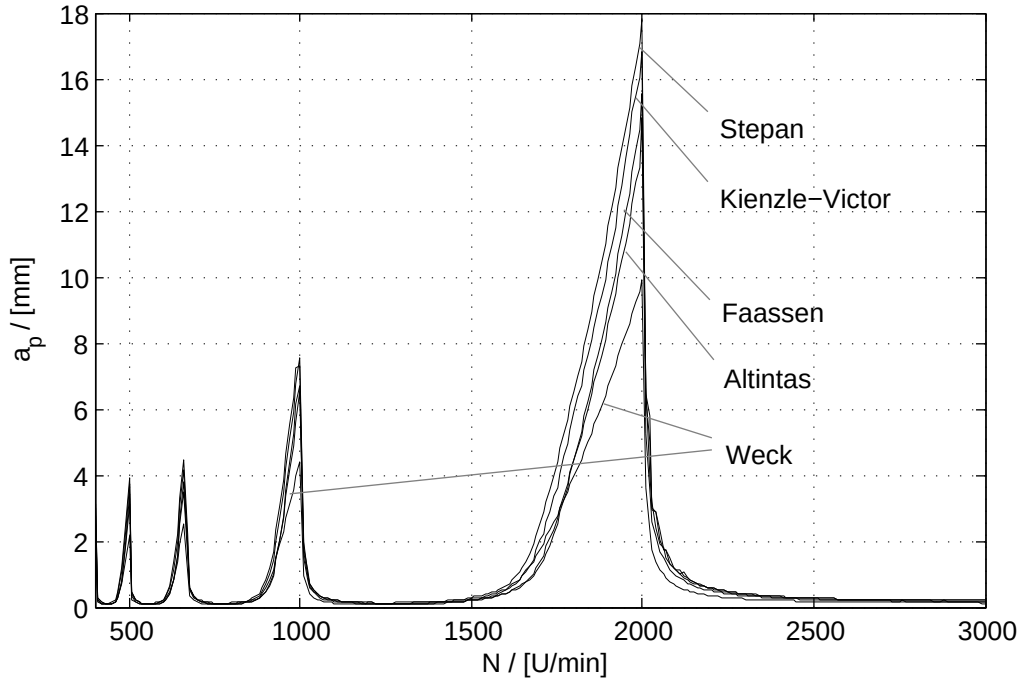

Figure 10: Comparison of the stability charts for $f_z = 0.45$ mm.

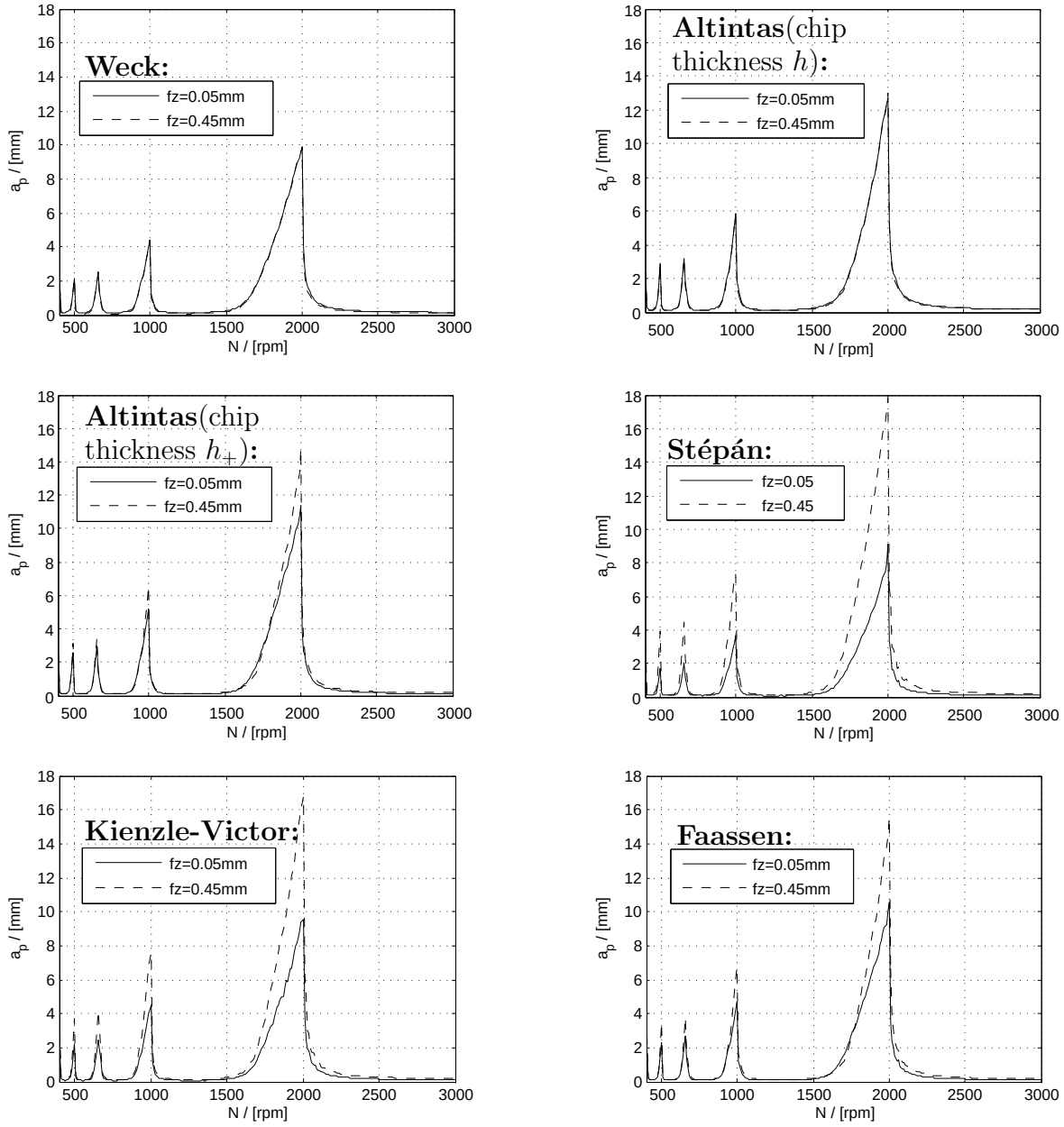

Figure 11: Detailed comparison of the stability charts showing the effect varying of f_z.

Hence the essential stability characteristics of the milling system investigated are reproduced independently of the chosen cutting force model. The cutting force models yield almost the same stability limit in the area between the peaks, as one can see in Figs. 9 and 10. Moreover, we note that for all models the stability limit rises continuously until the maximum is reached, decaying abruptly for further growth of the spindle speed. This seems to be another natural characteristic of the oscillation system investigated, displayed by every cutting force model.

We also detect differences between the predicted stability limits. Especially for spindle speeds close to N_1 - N_5 the variations are relatively large. Here, the stability peaks are of distinct height and width, depending on the cutting force model and on the feed per tooth. Since all peaks reveal the same deviations, it suffices to analyze only the largest peak, located around $N_1 = 2000$ rpm. Firstly, one notices the different scales of the abscissa in the diagrams for $f_z = 0.05$ mm and $f_z = 0.45$ mm. The overall maximum for the higher feed is about 1.7 times greater than that for the lower one. The difference proves that it is not admissible to neglect the effect of f_z. For $f_z = 0.05$ mm the maximum curve is given by Weck's cutting force model. The graph belonging to this model lies above the other curves for the whole range (1500 rm – 2000 rpm). The next stability limit curve below the graph of Weck is given by Altintas's model followed by that computed with Faassen's approach. The lowest stability limit curve, which is located under all other curves, is the stability limit calculated with Stépán's force model. For $f_z = 0.45$ mm the order of curves is the opposite way around. The maximum curve is given by Stépán's model, followed by the graphs computed with Faassen's and Altintas' approach. The lowest stability limit curve belongs to Weck's model. This clearly indicates, that depending on the cutting force model the effect of f_z is more or less crucial. In order to investigate the effect of f_z in detail, we compare the stability limit computed for $f_z = 0.05$ mm with that for $f_z = 0.45$ mm for each cutting force model separately. The results of this comparison are given in Fig. 11. The graphs belonging to Weck's and Altintas' model using the chip thickness h show that for these approaches increasing f_z has no effect. The stability limits coincide over the whole range of spindle speed. However, the replacement of h with h_+ in Altintas' model introduces an effect of f_z. Like all non-linear models, Altintas' model now shows an important growth of the stability peaks with increasing f_z. Among the non-linear models, Stépán's approach exhibits the strongest dependence on the feed per tooth. In the neighborhood of N_1 - N_5 the stability limit grows dramatically. For $f_z = 0.45$ mm the stability peak is more than two times higher as for $f_z = 0.05$ mm. Compared to Stépán, the models of Kienzle/Victor and Faassen show a weaker dependance on f_z.

4.3. **The effect of linearization.** The general strategy to investigate the stability of periodic solutions of linear and non-linear DDEs is to look at the behavior of small perturbations of these solutions. We assume that the solution consists of a periodic term ($u^0(t) = u^0(t-\tau)$) and a small perturbation ($u^P(t)$):

$$u(t) = u^0(t) + \varepsilon u^P(t). \tag{4.1}$$

As we shall see, the periodic part satisfies eq. (2.1) for $h = h_{stat}$. The fact that the perturbations $u^P(t)$ are small allows performing the stability analysis for the linearized eq. (2.1). In order to derive this linearization, we insert the cutting forces according to Faassen (cf. eq. (2.12)) into eq. (2.3):

$$\begin{bmatrix} F_x \\ F_y \end{bmatrix}(u) = \sum_{j=0}^{N_z-1} A^j(t) \begin{bmatrix} K_r h^{xf}(u) \\ K_t h^{xf}(u) \end{bmatrix} + \underbrace{A^j(t) \begin{bmatrix} K_{re} \\ K_{te} \end{bmatrix}}_{b^j(t)}; \tag{4.2}$$

where $b^j(t) = b^j(t-\tau)$. Then we perform a Taylor expansion of the expression above, which yields the linearized right hand side of eq. (2.1), if we neglect the second order term:

$$F(u) = F(u^0) + \varepsilon \cdot \frac{\partial}{\partial \varepsilon}\{F(u^0 + \varepsilon u^P)\}_{\varepsilon=0} + 0(\varepsilon^2) := F^{lin} + o(\varepsilon).$$

As usual, the notation $f(\varepsilon) = o(\varepsilon)$ means $\frac{f(\varepsilon)}{\varepsilon} \to 0$ for $\varepsilon \to 0$.

Thus we get the expression

$$F^{lin} = \tilde{C}(t) \begin{bmatrix} \frac{f_z}{x_f} \\ 0 \end{bmatrix} + \tilde{b}(t) + \tilde{C}(t)(u^p(t) - u^p(t-\tau)), \tag{4.3}$$

with a periodic matrix

$$\tilde{C}(t) = \tilde{C}(t-\tau) = \sum_{j=0}^{N_z-1} A^j(t) x_f (f_z \sin\varphi_j)^{x_f - 1} \begin{bmatrix} K_R \sin\varphi_j & K_R \cos\varphi_j \\ K_T \sin\varphi_j & K_T \cos\varphi_j \end{bmatrix} \tag{4.4}$$

and

$$\tilde{b}(t) = \tilde{b}(t-\tau) = \sum_{j=0}^{N_z-1} b^j(t). \tag{4.5}$$

Defining $D_1 = \begin{pmatrix} 2\xi_1\omega_1 & 0 \\ 0 & 2\xi_2\omega_2 \end{pmatrix}$ and $D_2 = \begin{pmatrix} \omega_1^2 & 0 \\ 0 & \omega_2^2 \end{pmatrix}$ we assume that $u = u^0 + \varepsilon u^p$ solves eq. (2.1) with linearized right hand side as expressed in (4.4). This yields

$$\ddot{u}_0 + \varepsilon\ddot{u}^p + D_1\ddot{u}_0 + \varepsilon D_1\dot{u}^p + D_2 u^0 + \varepsilon D_2 u^p = C(t) \begin{bmatrix} \frac{f_z}{x_r} \\ 0 \end{bmatrix} + b(t) + \varepsilon C(t)(u^p(t) - u^p(t-\tau)).$$

From this we infer that we can split the linearization of (2.1) into two equations. The first one is an inhomogeneous ODE which has the periodic solution $u^0(t)$:

$$\ddot{u}^0 + D_1\dot{u}^0 + D_2 u^0 = C(t) \begin{bmatrix} \frac{f_z}{x_f} \\ 0 \end{bmatrix} + b(t), \tag{4.6}$$

where $C(t) := \tilde{C}(t)/m_c$ and $b(t) := \tilde{b}(t)/m_c$. The right hand side of eq. (4.6) is equal to eq. (4.2) for $h = h_{stat} \neq h(u)$. This equation was derived for Faassen's cutting force model. If we set $b(t) = 0$, we get the corresponding expression for Stépán's model. The second one is a linear non-autonomous DDE which controls the stability of the periodic solution of eq. (4.6)

$$\ddot{u}^p + D_1\dot{u}^p + D_2 u^p = C(t)(u^p(t) - u^p(t-\tau)). \tag{4.7}$$

This equation is valid both for Faassen's and Stépán's cutting force models. The linearity of the cutting force models allows directly the splitting up of the equation of motion into an ODE for the periodic solution and a DDE for the perturbation. For Altintas' model one gets the corresponding equations setting $x_f = 1$ in eq. (4.4) and eq. (4.6). The equations for Weck's model are derived setting additionally $b(t) = 0$ in eq. (4.6).

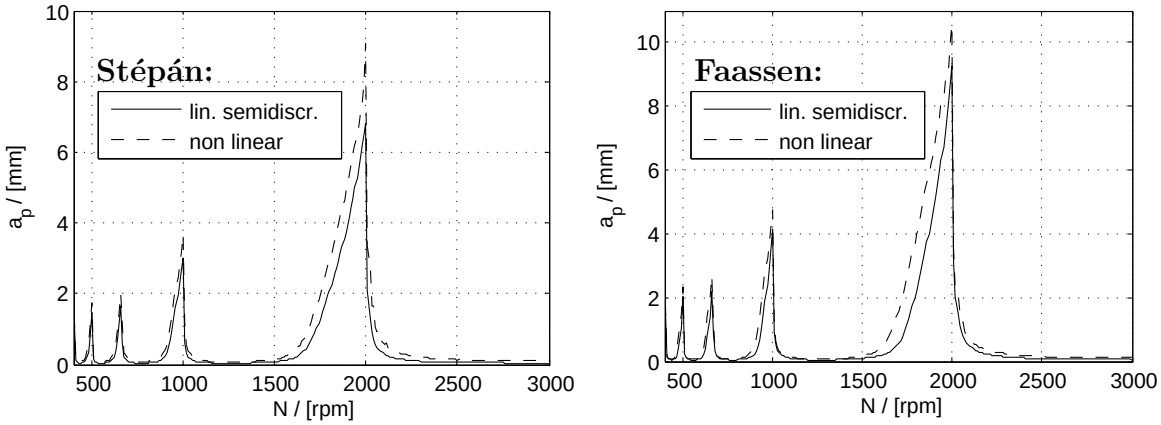

Figure 12: Detailed comparison of the stability charts of the non-linear and linearized models for $f_z = 0.05$ mm.

The fact that the linear cutting force models do not depend on f_z can be explained by looking at the derivation of eq. (4.7) for these models. Since the matrix $C(t)$ is independent of f_z the effect of f_z disappears.

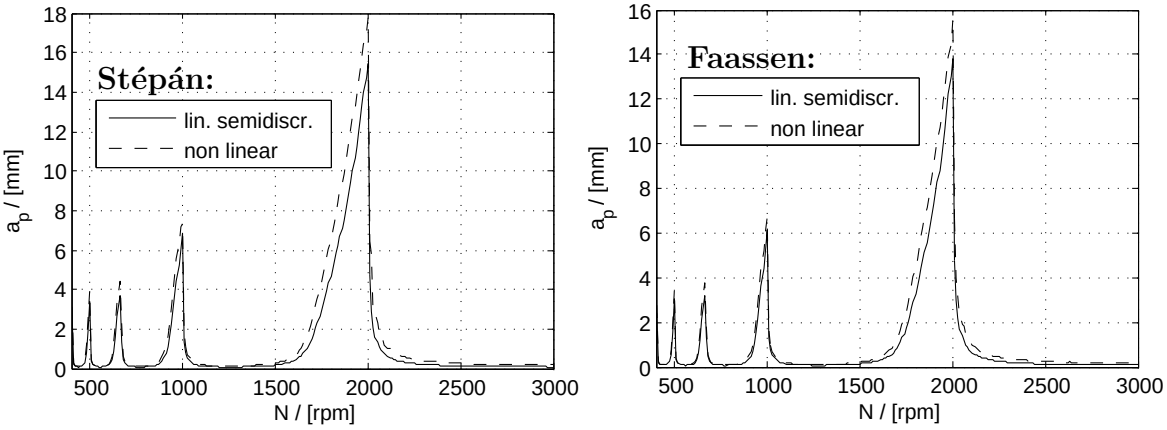

Figure 13: Detailed comparison of the stability charts of the non-linear and linearized models for $f_z = 0.45$ mm.

In principle one may compute the stability limit given by eq. (4.7) with the presented time domain simulation algorithm as shown for the 1D case. But in 2D the additional components C_{xy} and C_{yy} tend to infinity for $\varphi_j = 2k\pi$, $k = 0, 1, 2, \ldots$, leading to the failure of the chatter indicator η. This problem arises from the linearization, because the Taylor expansion of the right hand side of eq. (2.1) is not admissible for $h \to 0$. Hence, the time domain algorithm cannot be used in this case. Since Insperger's semi-discretization method uses time averaged values of $C(t)$ to calculate the stability limit, the difficulty can be overcome. The time

averaging smoothes out the peaks of $C(t)$ and one can expect even in this degenerate case reasonable results for the stability limit. Therefore we proceed as explained in the Appendix. In order to show the effect of linearization, we compare the stability limits computed with the linearized cutting force models with those we obtained from the non-linear ones. This means that the stability charts for the linearized equations were calculated with the semi-discretization approach, while the diagrams for the non-linear models were determined using the time domain algorithm. The comparison of non-linear and linearized models was carried out for two cutting force models (Stépán and Faassen) and two values of the feed per tooth ($f_z = 0.05$ mm and $f_z = 0.45$ mm). The results are presented in Fig. 12 and Fig. 13. The first observation is that the results of the linearized cutting force models lie slightly below the limits given by the non-linear ones. This seems to reflect a systematic difference between time-domain and Insperger's approach, already observed in Sect. 3.3. Besides, we can conclude that the linearized cutting force models provide the same stability limits as the non-linear ones, confirming thus the theoretical assumption that we can use the linearized equations, since the perturbations of the periodic solutions are small.

5. Conclusions

In the present paper we have developed a time domain simulation approach for the analysis of various popular linear and non-linear cutting force models. In order to show the effect of the cutting force model on the stability chart, a very simple milling system has been chosen. Stability charts have been calculated and compared to illustrate the effect of the cutting force model. Finally the non-linear models have been linearized, stability charts have been computed and compared to the results for the non-linear equations. The results show that each cutting force model is capable of reproducing the principal stability behavior of the investigated milling system. The main difference between the linear and non-linear cutting force models is the dependance on the feed per tooth f_z: While the non-linear models display an increasing stability limit for higher values of f_z, the linear ones are not dependent of the feed per tooth. In order to apply other, more faster stability analysis methods than time domain simulation, e.g. Insperger's semi-discretization method, one needs linear or linearized models. We have shown that the linearization does not change significantly the stability limits predicted by the fully non-linear models. It is therefore admissible to replace a non-linear cutting force expression with its linearized form, provided that one is interested in the accurate prediction of the stability limit of a milling process. However, if one searches for an exact representation of the cutting force in time, the use of a non-linear model, which takes into account the most important characteristics of the cutting process, is recommended.

Further research is necessary to investigate the effect of the initial conditions. The threshold η^{th} to distinguish stable form unstable cutting conditions may change if the initial conditions are modified. Other tasks are the development of an improved multi body system to capture the machine dynamics and a study of the influence of workpiece stiffness on the stability analysis.

References

1. Y. Altintas, *Manufacturing automation*, Cambridge University Press, 2000.
2. M. L. Campomanes and Y. Altintas, *An improved time doman simulation for dynamic milling at small radial immersions*, Journal of Manufacturing Science and Engineering (2003).
3. R. P. H. Faassen, N. van de Wouw, J.A.J. Oosterling, and H. Nijmeijer, *Prediction of regenerative chatter by modelling and analysis of high-speed milling*, International Journal of Machine Tools and Manufacture (2003).
4. M. Farkas, *Periodic motions*, Applied Mathematical Sciences, vol. 104, Springer, New York, 1994.
5. J. K. Hale and S. M. Verduyn Lunel, *Introduction to functional-differential equations*, Applied Mathematical Sciences, vol. 99, Springer, New York, 1993.
6. T. Insperger, *Stability analysis of periodic delay-differential equations modeling machine tool chatter*, Ph.D. thesis, Budapest University of Technology and Economics, 2002.
7. T. Insperger and G. Stépán, *Stability of the milling process*, Periodica Polytechnica Service Mechanical Engineering (1999).
8. ———, *Updated semi-discretization method for periodic delay-differential equations with discrete delay*, International Journal for Numerical Methods in Engineering (2004).
9. V. Lakshmikantham and D. Trigiante, *Theory of difference equations*, Mathematics in Science and Engineering, vol. 181, Academic Press Inc., Boston, MA, 1988, Numerical methods and applications.
10. H. Z. Li and X. P. Li, *Modeling and simulation of chatter in milling using a predictive force model*, International Journal of Machine Tools and Manufacture (2000).
11. ———, *Modeling of cutting forces in helical end milling using a predictive machining theory*, International Journal of Mechanical Sciences (2001).
12. H. Z. Li, X. P. Li, and X. Q. Chen, *A novel chatter stability criterion for the modelling and simulation of the dynamic milling process in the time domain*, International Journal of Advanced Manufacturing Technologies (2003).
13. P. L. B. Oxley, *The mechanics of machining*, Ellis Horwood series in mechanical engineering, 1977.
14. L. F. Shampine and S. Thompson, *Solving ddes in matlab*, Applied Numerical Mathematics (2001).
15. N. D. Sims, *The self-excitation damping ratio: a chatter criterion for time-domain milling simulations*, Journal of Manufacturing Science and Engineering (2005).
16. S. Smith and J. Tlusty, *Efficient simulation programs for chatter in milling*, Annals of the CIRP (1993).
17. G. Stépán, *Retarded dynamical systems: stability and characterisitc functions*, Pitman Research Notes in Mathematics Series, 1989.
18. T. Suhrmann, M. Kalveram, and K. Weinert, *Simulation of cutting tool vibrations for the milling of free formed surfaces*, Proceedings of the 8th CIRP International Workshop on Modeling of Machining Operations, 2005.
19. J. Tlusty, *Manufacturing processes and equipement*, Prentic Hall, 2000.
20. S. A. Tobias, *Schwingungen an Werkzeugmaschinen*, Carl Hanser Verlag München, 1961.
21. H. K. Tönshoff and B. Denkena, *Spanen*, Springer, 2004.
22. M. Weck and K. Teipel, *Dynamisches Verhalten spanender Werkzeugmaschinen*, Springer Berlin Heidelberg New York, 1977.

6. Appendix – Updated semi-discretization method

For the reader's convenience we recall the semi-discretization method, which have been used in section 3 and 4.3. Following the lines of Insperger [8], we consider the n-dimensional delay differential equation:

$$\dot{x}(t) = A(t)x(t) + B(t)x(t-\tau), \text{ where } A(t+T) = A(t),\ B(t+T) = B(t), \tag{6.1}$$

with the time delay τ and the time period T. For milling systems with fixed spindle speed $\tau = T$. The first step of semi-discretization is the construction of the time interval division $[t_i, t_{i+1}]$ of length Δt, $i = 0, 1, \ldots$ so that $T = k\Delta t$, where k is an integer that can be considered as an approximation parameter regarding the time period.

Introduce the integer m so that:

$$m = \text{int}\left(\frac{\tau + \Delta t/2}{\Delta t}\right), \tag{6.2}$$

where $int()$ is the function that rounds positive numbers towards zero (e.g. int(4.82) = 4). The integer m can be considered as an approximation parameter regarding time delay.

Use the notation $x(t_j) = x_j$ for any integer j. In the ith interval, eq. (6.1) can be approximated as:

$$\dot{x}(t) = A_i x(t) + B_i x_{\tau,i}, \tag{6.3}$$

where:

$$A_i = \frac{1}{\Delta t}\int_{t_i}^{t_{i+1}} A(t)d\tau,\ B_i = \frac{1}{\Delta t}\int_{t_i}^{t_{i+1}} B(t)d\tau, \tag{6.4}$$

and x_τ is the following approximation of the delayed term:

$$x(t-\tau) \approx x(t_i + \Delta t/2 - \tau) \approx w_b x_{i-m} + w_a x_{i-m+1} = x_{\tau,i}, \tag{6.5}$$

where the weights of x_{i-m} and x_{i-m+1} are:

$$w_b = \frac{\tau + \Delta t/2 - m\Delta t}{\Delta t}, \tag{6.6}$$

$$w_a = \frac{m\Delta t + \Delta t/2 - \tau}{\Delta t}. \tag{6.7}$$

The delayed term is approximated as a weighted linear combination of the delayed discrete values x_{i-m} and x_{i-m+1}. With the help of the usual Langrange remainder term, an error estimation can be constructed in the usual way for this natural choice of weights.

The solution of eq. (6.3) for the initial condition $x(t_i) = x_i$ reads:

$$x(t) = \exp(A_i(t-t_i))\left(x_i + A_i^{-1}B_i x_{\tau,i}\right) - A_i^{-1}B_i x_{\tau,i}\,. \tag{6.8}$$

Substituting $t = t_{i+1}$ and using equation (6.5), $x_{i+1} = x(t_{i+1})$ is defined as:

$$x_{i+1} = P_i x_i = w_a, R_i x_{i-m+1} + w_b R_i x_{i-m}, \tag{6.9}$$

where:

$$P_i = \exp(A_i\Delta t),$$
$$R_i = (\exp(A_i\Delta t) - I)A_i^{-1}B_i\,.$$

Here, I denotes identity matrix.

Now, according to eq. (6.9), a discrete map can be defined:

$$y_{i+1} = C_i y_i, \tag{6.10}$$

where the $n(m+1)$-dimensional vector is $y_i = \text{col}(x_i,\ x_{i-1}, \ldots,\ x_{i-m})$ and the coefficient matrix has the form:

$$C_i = \begin{pmatrix} P_i & 0 & 0 & \dots & 0 & w_a R_i & w_b R_i \\ I & 0 & 0 & \dots & 0 & 0 & 0 \\ 0 & I & 0 & \dots & 0 & 0 & 0 \\ \vdots & \vdots & \ddots & \ddots & \vdots & \vdots & \vdots \\ 0 & 0 & 0 & \ddots & 0 & 0 & 0 \\ 0 & 0 & 0 & \dots & I & 0 & 0 \\ 0 & 0 & 0 & \dots & 0 & I & 0 \end{pmatrix}. \tag{6.11}$$

The next step is to determine the transition matrix ϕ over the principal period $T = k\Delta t$. This serves a finite-dimensional approximation of the monodromy operator in the infinite-dimensional version of the Floquet theory [5, 4]. The transition matrix gives the connection between y_0 and y_k in the form:

$$y_k = \phi y_0, \tag{6.12}$$

where ϕ is given by coupling the solutions:

$$\phi = C_{k-1} C_{k-2} \dots C_1 C_0. \tag{6.13}$$

Now, the stability investigation is reduced to the problem, whether the eigenvalues of ϕ are in modulus less than one [9].